Microgrid Clusters Control with Unknown Network and Load Parameters

Mikhak Samadi
Electrical Engineering
Hydro Ottawa
Ottawa, Canada
mikhaksamadi@hydroottawa.com

Nan Chen
Electrical Eng. & Comp. Sci.
University of Ottawa
Ottawa, Canada
nchen@uottawa.ca

Javad Fattahi
Electrical Eng. & Comp. Sci.
University of Ottawa
Ottawa, Canada
javad.fattahi@uottawa.ca

***Abstract*—This paper presents a distributed nonlinear adaptive control framework for voltage-frequency regulation and current (or power) sharing in an AC microgrid (MG) cluster, where multiple MGs are interconnected through resistive-inductive-capacitive (RLC) distribution lines of arbitrary topology. Each MG contains several parallel-connected distributed generation units (DGUs) interfaced by converters and supplies nonlinear ZIE (impedance-current-exponential) loads. The controller is formulated in the synchronous dq frame and explicitly accounts for unknown network and load parameters as well as plug-and-play (PnP) operations and line contingencies. In each MG, one DGU operates in grid-forming mode to regulate the bus voltage, and the remaining DGUs operate in grid-feeding mode to track current (or power) references that enforce proportional sharing. An adaptive backstepping design with Lyapunov analysis guarantees asymptotic voltage-frequency regulation and proportional sharing under the ZIE load model. Simulation results under load disturbances, PnP events, and unknown network reconfigurations illustrate the effectiveness and robustness of the proposed approach.**

***Index Terms*—microgrid cluster, adaptive backstepping control, ZIE load.**

I. Introduction

In recent years, alternating current (AC) microgrids (MGs) have emerged as a cornerstone of modern distribution systems, driven by the proliferation of converter-interfaced renewable sources, storage, and advanced control hardware [1]. AC MGs integrate distributed generation units (DGUs) such as photovoltaic panels, wind turbines and storages, typically via voltage-source converters (VSCs) with LC or LCL filters, and can operate in both grid-connected and islanded modes. Their ability to enhance reliability, resilience, and power quality while supporting bidirectional power flow makes them key enablers of future smart grids [2]. Parallel operation of multiple DGUs at a bus is widely used to overcome power limitations of individual converters and increase redundancy. However, parallel operation can cause overloading and power-quality degradation, making coordinated voltage-frequency regulation and power sharing crucial.

To increase flexibility and resilience, multiple MGs can be interconnected into an AC MG cluster through resistive-inductive-capacitive (RLC) distribution lines with arbitrary topology. In such clusters, the MGs interact dynamically through line currents and bus voltages, and the network is often subject to PnP operation and topology changes. Centralized control schemes based on a supervisory controller and global information [3] can, in principle, address these interactions, but they suffer from scalability and reliability limitations due to their dependence on communication networks and accurate global models.

Distributed and decentralized control frameworks have therefore received significant attention [4]. Droop-based control is the most common primary mechanism for grid-forming converters because of its simplicity and communication-free design [1]. However, conventional droop schemes face several challenges. They incur steady-state voltage and frequency deviations and may share reactive power inaccurately under mismatched line impedances. Moreover, they can exhibit degraded transient performance under dynamic conditions or nonlinear loads [5]. Various improvements have been proposed based on virtual impedance, secondary control layers, and adaptive gains [6]–[8], but many of these designs rely on simplified quasi-steady models and neglect inner-loop and network dynamics.

Non-droop-based strategies have been investigated to overcome these drawbacks, including event-triggered, model predictive, robust, and adaptive controllers [9], [10]. While these methods improve dynamic performance and robustness, they often assume known or slowly varying line parameters and idealized load models. In particular, the effects of resistive-inductive (RL) line dynamics and their coupling with converter filters are frequently simplified [11]. Moreover, many works focus on constant impedance (Z) or constant current (I) loads, whereas practical AC networks increasingly include nonlinear exponential (E) loads such as motor drives and converter-fed appliances that exhibit negative incremental impedance and can reduce system damping [12], [13]. This combination of uncertain network parameters, complex load behavior, and PnP network operation motivates nonlinear control methods that explicitly handle large-signal dynamics and significant parametric uncertainty.

The main contributions of this work are: (i) An adaptive control framework for AC MG clusters. The framework can adapt to arbitrary topology and RLC line dynamics with parallel operation of DGUs to supply nonlinear ZIE (impedance–current–exponential) loads. To the best of our

979-8-3315-8138-1

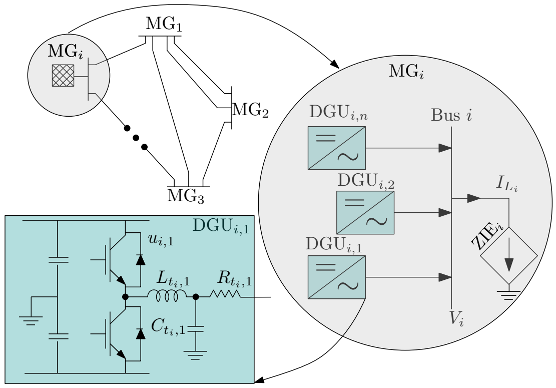

Fig. 1: A typical AC microgrid (MG) cluster contains several DGUs supplying ZIE loads

knowledge, this is the first nonlinear adaptive controller for AC MG clusters explicitly treating ZIE-type loads. (ii) Guaranteed large-signal voltage-frequency regulation and accurate current (or power) sharing under fully unknown network and load parameters, via online identification of aggregated ZIE-type regressors. (iii) A fully decentralized implementation that uses only local measurements, does not rely on line parameters, and requires no inter-MG communication, thereby supporting PnP operation and robustness to line failures and network reconfigurations.

II. Dynamic model of AC MG cluster system

Consider an isolated AC MG cluster consisting of N MGs interconnected by M distribution lines, as shown in Fig. 1. MG i contains n_i parallel DGUs, all tied to a common AC bus that supplies a local ZIE load. In the synchronous dq frame, let J denote the 90° rotation matrix. The corresponding block-diagonal matrices for buses and lines are $\mathbb{J}_N = I_N \otimes J$ and $\mathbb{J}_M = I_M \otimes J$, respectively. Let $\mathcal{A} \in \mathbb{R}^{N\times M}$ be the incidence matrix of the network, and define its dq-stacked form as

$$\mathcal{A}_2 = \mathcal{A} \otimes I_2 \in \mathbb{R}^{2N\times 2M}. \tag{1}$$

Line and bus energy-storage parameters are assumed isotropic in dq. We also assume a voltage lower bound $\|v_i(t)\| \geq V_{\min} > 0$ for all i and t so that the ZIE load terms are well defined.

Each distribution line k is modeled as a series RL element in the dq frame:

$$L_k \dot{i}_k = -R_k i_k + \omega_0 L_k J i_k + \sum_{i=1}^{N} \mathcal{A}_{ik} v_i, \tag{2}$$

where $i_k \in \mathbb{R}^2$ is the line current, $v_i \in \mathbb{R}^2$ is the bus voltage of MG i, and $\mathcal{A}_{ik} \in \{-1, 0, 1\}$ encodes the line orientation.

In MG i, let $v_i = [v_{d_i}\ v_{q_i}]^T$ be the bus voltage and $i_{t_{i,j}} = [i_{d_{i,j}}\ i_{q_{i,j}}]^T$ be the inductor current of DGU (i,j). The total converter current injected into the bus is

$$i_{o_i} = \sum_{j=1}^{n_i} i_{t_{i,j}}. \tag{3}$$

The bus capacitor dynamics are

$$C_{t_i} \dot{v}_i = i_{o_i} - \sum_{k=1}^{M} \mathcal{A}_{ik} i_k - i_{L_i}(v_i) + \omega_0 C_{t_i} J v_i, \tag{4}$$

where C_{t_i} is the lumped shunt capacitance of MG i.

Each DGU is modeled as a VSC with an L-filter. Its inductor dynamics are

$$L_{t_{i,j}} \dot{i}_{t_{i,j}} = -R_{t_{i,j}} i_{t_{i,j}} - v_i + e_{i,j} m_{i,j} + \omega_0 L_{t_{i,j}} J i_{t_{i,j}}, \tag{5}$$

where $m_{i,j} = [m_{d_{i,j}}\ m_{q_{i,j}}]^T$ is the modulation (control) vector and $e_{i,j}$ is the DC-link voltage.

The ZIE load at bus i is modeled as

$$\begin{aligned} i_{L_i}(v_i) &= G_{l_i} v_i + i_{l_i} \\ &\quad + E_{p_i} \left(\frac{\|v_i\|}{V_0}\right)^{n_{p_i}-2} v_i + E_{q_i} \left(\frac{\|v_i\|}{V_0}\right)^{n_{q_i}-2} J v_i, \end{aligned} \tag{6}$$

where $G_{l_i} \geq 0$ is the conductance component, $i_{l_i} \in \mathbb{R}^2$ is the constant-current component, and E_{p_i}, E_{q_i} with exponents n_{p_i}, n_{q_i} capture the exponential (E) load terms; $V_0 > 0$ is a known reference voltage.

Stack line currents, bus voltages, and MG injections can be expressed in compact form as

$$I = [i_1^T\ \ldots\ i_M^T]^T \in \mathbb{R}^{2M}, \tag{7a}$$

$$V = [v_1^T\ \ldots\ v_N^T]^T \in \mathbb{R}^{2N}, \tag{7b}$$

$$I_o = [i_{o_1}^T\ \ldots\ i_{o_N}^T]^T \in \mathbb{R}^{2N}. \tag{7c}$$

Let I_t collect all DGU currents and m be all modulation vectors. Define the block-diagonal matrices $L := \mathrm{diag}\{L_k I_2\}$, $R := \mathrm{diag}\{R_k I_2\}$, and $\mathcal{C}_t := \mathrm{diag}\{\mathcal{C}_{t_i} I_2\}$, and define similarly Γ_t, $\mathcal{R}_t$, and Ξ for the per-DGU parameters as in (5). Let $\mathbb{I}$ be the summation map such that $I_o = \mathbb{I} I_t$, and stack the ZIE loads as

$$I_L(V) = [i_{L_1}(v_1)^T\ \ldots\ i_{L_N}(v_N)^T]^T. \tag{8}$$

The complete MG cluster dynamics can then be written as

$$L\dot{I} = -RI + \omega_0 L \mathbb{J}_M I + \mathcal{A}_2^T V, \tag{9a}$$

$$\mathcal{C}_t \dot{V} = I_o - \mathcal{A}_2 I - I_L(V) + \omega_0 \mathcal{C}_t \mathbb{J}_N V, \tag{9b}$$

$$\dot{I}_o = -\mathbb{I}\Gamma_t \mathbb{I}^T V - \mathbb{I}\mathcal{R}_t I_t + \mathbb{I}\Xi m + \omega_0 \mathbb{J}_N I_o. \tag{9c}$$

These equations form the basis for the control design in the next section. In microgrid i, converter $\mathrm{DGU}_{i,1}$ operates in grid forming mode and regulates the local bus voltage and frequency. The remaining DGUs operate in grid feeding mode and regulate their output currents or powers in order to achieve proportional sharing.

Let $v_i = [v_{d_i}\ v_{q_i}]^T$ denote the bus voltage at MG i. The desired steady-state bus voltage is

$$v_i^* = [V_i^*\ 0]^T, \qquad V_i^* \geq V_{\min} > 0. \tag{10}$$

The first objective is that $v_i(t)$ converges to v_i^* for every MG i, so that the bus voltage magnitude and frequency are regulated at the prescribed values.

Let $i_{t_{i,j}} = [i_{d_{i,j}}\ i_{q_{i,j}}]^T$ denote the inductor current of DGU (i,j) and

$$i_{o_i} = \sum_{j=1}^{n_i} i_{t_{i,j}} \tag{11}$$

be the total converter current injected into bus i. Let $P_i = \mathrm{diag}\{\rho_{i,1}, \ldots, \rho_{i,n_i}\}$ with strictly positive weights $\rho_{i,j} > 0$. Denote by $i_{o_i}^\star$ the steady-state injection at MG i that is consistent with the cluster equilibrium at $V^* = [v_1^{*T}\ \ldots\ v_N^{*T}]^T$

979-8-3315-8138-1

under the ZIE loads and line dynamics of Section II. The desired steady-state DGU currents are

$$i^\star_{t_{i,j}} = \frac{\rho_{i,j}}{\mathbf{1}^T_{n_i} P_i \mathbf{1}_{n_i}} i^\star_{o_i}, \qquad j = 1, \ldots, n_i. \tag{12}$$

The second objective is that $i_{t_{i,j}}(t)$ converges to $i^\star_{t_{i,j}}$ for all DGUs, so that the net injection $i^\star_{o_i}$ at each bus is shared in proportion to the weights $\rho_{i,j}$.

If it is more convenient to prescribe proportional sharing in terms of active and reactive powers, let $p^\star_{i,j}$ and $q^\star_{i,j}$ be the desired steady-state powers for DGU (i, j) and define the total active and reactive powers at bus i as $p^\star_{o_i} = \sum_{j=1}^{n_i} p^\star_{i,j}$ and $q^\star_{o_i} = \sum_{j=1}^{n_i} q^\star_{i,j}$, respectively. Thus, proportional power sharing can be written as

$$p^\star_{i,j} = \frac{\rho_{i,j}}{\mathbf{1}^T_{n_i} P_i \mathbf{1}_{n_i}} p^\star_{o_i}, \tag{13a}$$

$$q^\star_{i,j} = \frac{\rho_{i,j}}{\mathbf{1}^T_{n_i} P_i \mathbf{1}_{n_i}} q^\star_{o_i}. \tag{13b}$$

In the dq frame the instantaneous active and reactive powers associated with voltage v and current i are $p = v^T i$ and $q = v^T J i$. Evaluated at $v^*_i = [V^*_i \ 0]^T$, the steady-state current reference associated with the power target $(p^\star_{i,j}, q^\star_{i,j})$ is

$$i^\star_{t_{i,j}} = \frac{1}{\|v^*_i\|^2} \left(p^\star_{i,j} v^*_i - q^\star_{i,j} J v^*_i \right), \tag{14}$$

which satisfies $v^{*T}_i i^\star_{t_{i,j}} = p^\star_{i,j}$ and $v^{*T}_i J i^\star_{t_{i,j}} = q^\star_{i,j}$. The mapping in (14) is well defined because $\|v^*_i\| = V^*_i \geq V_{\min}$.

III. Control design

In each MG i, the unit $\mathrm{DGU}_{i,1}$ operates in grid forming mode and regulates the local bus voltage. The remaining DGUs operate in grid feeding mode and regulate their output currents so that the proportional sharing pattern (12) is achieved. All control laws use only measurements within MG i. No inter MG communication is required and no line parameters are used. Let I^* denote the steady-state line current vector consistent with V^* and the ZIE loads, and define error variables as

$$\tilde{I} = I - I^*, \tag{15a}$$

$$\tilde{V} = V - V^*, \tag{15b}$$

$$\tilde{I}_o = I_o - \xi, \tag{15c}$$

$$\tilde{I}_{t_{i,j}} = I_{t_{i,j}} - \hat{I}^*_{t_{i,j}}, \tag{15d}$$

where $\xi \in \mathbb{R}^{2N}$ is a virtual input and $\hat{I}^*_{t_{i,j}}$ is an estimate of the desired steady-state current $i^\star_{t_{i,j}}$ in (12). The estimate is constructed from an estimate of the steady-state bus injection:

$$\hat{I}^\star_o = \Omega(V^*) \hat{\mathcal{Q}}, \tag{16a}$$

$$\hat{I}^*_{t_{i,j}} = \frac{\rho_{i,j}}{\mathbf{1}^T_{n_i} P_i \mathbf{1}_{n_i}} \hat{I}^\star_{o_i}, \tag{16b}$$

where $\hat{\mathcal{Q}}$ is the estimate of the stacked ZIE parameter vector $\mathcal{Q}$ defined in Section II and $\Omega(V)$ is the corresponding block diagonal regressor. As in Section II, the aggregate effect of ZIE loads and steady network injections can be written as

$$I_L(V) + \mathcal{A}_2 I^* = \Omega(V) \mathcal{Q}. \tag{17}$$

The first backstepping step treats I_o as a virtual input for the bus dynamics and uses the Lyapunov function

$$W_1 = \frac{1}{2} \tilde{V}^T \mathcal{C}_t \tilde{V} + \frac{1}{2} \tilde{I}^T L \tilde{I} + \frac{1}{2} \tilde{\mathcal{Q}}^T \Lambda_1 \tilde{\mathcal{Q}}, \tag{18}$$

with $\tilde{\mathcal{Q}} = \mathcal{Q} - \hat{\mathcal{Q}}$ and $\Lambda_1 \succ 0$. Following the adaptive backstepping construction in [14], [15], the virtual input and the parameter update are chosen as

$$\xi = -K_1 \tilde{V} + \Omega(V) \hat{\mathcal{Q}}, \tag{19a}$$

$$K_1 = \mathrm{blkdiag}(\kappa_{1,1} I_2, \ldots, \kappa_{1,N} I_2), \tag{19b}$$

$$\dot{\hat{\mathcal{Q}}}_i = -\Lambda^{-1}_{1,i} \Omega_i(v_i)^T \tilde{v}_i, \tag{19c}$$

where $\kappa_{1,i} > 0$ and $\Lambda_{1,i} \succ 0$ are design parameters. With (19), the derivative of W_1 is negative semidefinite up to terms that depend on $\tilde{I}_o$ and the DGU currents and is therefore suitable for the next backstepping step.

In the second step, the physical modulation inputs $m_{i,j}$ are constructed so that $\tilde{I}_o$ and $\tilde{I}_{t_{i,j}}$ converge to zero while preserving the adaptive structure. Let $U = \mathbb{I}\hat{\Xi} m$ with $U = [U_1^T \ldots U_N^T]^T$ and $U_i = \mathbf{1}^T_{n_i} \hat{\Xi}_i m_i$, and let $\hat{\Gamma}_{t_{i,j}}$, $\hat{\mathcal{R}}_{t_{i,j}}$, $\hat{\Xi}_{i,j}$, and $\hat{\mathcal{C}}^{-1}_{t_i}$ denote estimates of the corresponding electrical parameters. The backstepping construction yields the following aggregated current reference at MG i

$$\begin{aligned} U_i = &-\kappa_{2,i}(t) \tilde{I}_{o_i} - \tilde{V}_i + \mathbf{1}^T_{n_i} \hat{\Gamma}_{t_i} \mathbf{1}_{n_i} V_i + \mathbf{1}^T_{n_i} \hat{\mathcal{R}}_{t_i} I_{t_i} \\ &- \left(\kappa_{1,i} I_2 - \frac{\partial (\Omega_i(v_i) \hat{\mathcal{Q}}_i)}{\partial v_i} \right) \left(\hat{\mathcal{C}}^{-1}_{t_i} I_{o_i} - \Omega_i(v_i) \hat{\mathcal{Q}}_{c_i} \right) \\ &+ \Omega_i(v_i) \dot{\hat{\mathcal{Q}}}_i, \end{aligned} \tag{20}$$

where $\kappa_{2,i}(t) > 0$ is a time varying damping gain and $\hat{\mathcal{Q}}_{c_i}$ collects scaled load parameters.

For the current controlled DGUs $j = 2, \ldots, n_i$ the modulation inputs are chosen as

$$\begin{aligned} m_{i,j} = \hat{\Xi}^{-1}_{i,j} \Big(&- k_{i,j} \tilde{I}_{t_{i,j}} + \hat{\Gamma}_{t_{i,j}} V_i + \hat{\mathcal{R}}_{t_{i,j}} I_{t_{i,j}} \\ &+ \frac{\rho_{i,j}}{\mathbf{1}^T_{n_i} P_i \mathbf{1}_{n_i}} \Omega_i(v^*_i) \dot{\hat{\mathcal{Q}}}_i \Big), \end{aligned} \tag{21}$$

with $k_{i,j} > 0$. The grid forming DGU uses

$$\begin{aligned} m_{i,1} = \hat{\Xi}^{-1}_{i,1} \Big(&- \kappa_{2,i}(t) \tilde{I}_{o_i} - \tilde{V}_i + \hat{\Gamma}_{t_{i,1}} V_i + \hat{\mathcal{R}}_{t_{i,1}} I_{t_{i,1}} \\ &- \left(\kappa_{1,i} I_2 - \frac{\partial (\Omega_i(v_i) \hat{\mathcal{Q}}_i)}{\partial v_i} \right) \left(\hat{\mathcal{C}}^{-1}_{t_i} I_{o_i} - \Omega_i(v_i) \hat{\mathcal{Q}}_{c_i} \right) \\ &+ \sum_{j=2}^{n_i} k_{i,j} \tilde{I}_{t_{i,j}} + \left(\Omega_i(v_i) - \frac{\sum_{j=2}^{n_i} \rho_{i,j}}{\mathbf{1}^T_{n_i} P_i \mathbf{1}_{n_i}} \Omega_i(v^*_i) \right) \dot{\hat{\mathcal{Q}}}_i \Big). \end{aligned} \tag{22}$$

The parameter estimates are updated by gradient type laws of the form:

$$\dot{\hat{\mathcal{Q}}}_{c_i} = -\Lambda^{-1}_{2,i} \phi_{\mathcal{Q}_i}(\tilde{I}_{o_i}, v_i), \tag{23a}$$

$$\dot{\hat{\mathcal{C}}}^{-1}_{t_i} = \lambda^{-1}_{3,i} \phi_{C_i}(\tilde{I}_{o_i}, I_{o_i}, v_i), \tag{23b}$$

$$\dot{\hat{\Gamma}}_{t_{i,j}} = -\mu^{-1}_{1_{i,j}} \phi_{\Gamma_{i,j}}(\tilde{I}_{o_i}, \tilde{I}_{t_{i,j}}, V_i), \tag{23c}$$

$$\dot{\hat{\mathcal{R}}}_{t_{i,j}} = -\mu^{-1}_{2_{i,j}} \phi_{R_{i,j}}(\tilde{I}_{o_i}, \tilde{I}_{t_{i,j}}, I_{t_{i,j}}), \tag{23d}$$

$$\dot{\hat{\Xi}}_{i,j} = \mu^{-1}_{3_{i,j}} \phi_{\Xi_{i,j}}(\tilde{I}_{o_i}, \tilde{I}_{t_{i,j}}, m_{i,j}), \tag{23e}$$

where $\Lambda_{2,i} \succ 0$, $\lambda_{3,i} > 0$, and $\mu_{1_{i,j}}, \mu_{2_{i,j}}, \mu_{3_{i,j}} > 0$ are design gains and the regression vectors $\phi.(\cdot)$ follow from the

979-8-3315-8138-1

TABLE I: Simulation scenarios used in the case studies.

Case ID	Description
Case 1	Plug-and-play: DGUs added/removed during the run.
Case 2	Load sharing using ZIE-based adaptive weights.
Case 3	Topology changes and contingencies unknown.

construction of the stepping backward. Projection is used so that $\hat{\Xi}_{i,j}$ and $\hat{\mathcal{C}}_{t_i}^{-1}$ remain bounded and strictly positive.

The time varying damping gains $\kappa_{2,i}(t)$ are chosen to dominate the cross couplings between line currents and injection currents. Following [16], a convenient choice is

$$\kappa_{2,i}(t) = \eta_i + \theta_i \Big\| \Big(-\kappa_{1,i} I_2 + \frac{\partial(\Omega_i(v_i)\hat{\mathcal{Q}}_i)}{\partial v_i} \Big) C_{\min,i}^{-1} \Big\|^2, \tag{24}$$

where $\eta_i > 0$ is a constant, $C_{\min,i} := \sum_{j=1}^{n_i} C_{\min,i,j}$ with $C_{\min,i,j}$ as a known positive lower bound for the capacitance seen at bus i, and

$$\theta_i = \sum_{k\in\mathcal{E}_{\max,i}} \frac{1}{2}\gamma_k. \tag{25}$$

Here $\mathcal{E}_{\max,i}$ is the set of distribution lines incident to bus i, γ_k are positive constants that satisfy $\gamma_k > R_{\min,k}^{-1}$, and $R_{\min,k}$ are known positive lower bounds for the line resistances R_k. With this choice, the coupling terms generated by the network interconnections can be upper bounded by the dissipative terms in the derivative of the Lyapunov function. The stability property of the closed-loop AC dq-frame system can be shown under the controller and adaptation laws. A Lyapunov function W is constructed by adding to W_1 in (18) quadratic terms in the current-tracking errors $\tilde{I}_o$ and $\tilde{I}_{t_{i,j}}$ and quadratic terms in all parameter-estimation errors that appear in (19), (20), (21), and (23).

IV. Simulation Results

The cluster comprises $N = 10$ microgrids (MGs), each represented as a bus in a connected AC network and interconnected by $M = 15$ RL distribution lines. The line set corresponds to a sparse, undirected graph whose adjacency list is defined in the simulation code; all line resistances and inductances are known to the plant model but never used by the controller. Each MG i hosts $n_i = 3$ parallel converter-interfaced DGUs, all equipped with identical L-filters with inductance $L = 1.8 \times 10^{-3}\,$H, series resistance $R = 0.12\,\Omega$, and a lumped shunt capacitance $\mathcal{C}_{t_i} = C = 2.5\times10^{-3}\,$F. All converter and network dynamics are modeled in the synchronous dq reference frame with nominal frequency $\omega_0 = 2\pi \times 60\,\mathrm{rad/s}$. The G_{l_i}, b_i, E_{p_i}, and E_{q_i} are unknown constants.

Figures 2 shows the controller's behavior under Cases 1–3 in Table I. In the proportional sharing scenario (Case 1), Figure 2a shows the fractional current shares achieved by the DGUs on three representative buses. After a short transient, each fraction converges to a constant level determined by the local weights $\rho_{i,j}$, and the traces remain essentially flat for the rest of the run. The fact that the fractions settle without oscillations, despite the nonlinear ZIE terms, reflects that the unknown load contributions appear only in the aggregated regressor $\Omega(V)\mathcal{Q}$ and therefore do not explicitly enter the derivative of the Lyapunov function W. The global error envelope in Figure 2b shows the norm of the current error $|I_{\mathrm{ach}} - I^{\star}|$ over time, with a clear initial peak followed by a fast decay and a slow convergence plateau. This behavior is typical of adaptive backstepping schemes, where state errors decay faster than parameter estimates, and is consistent with the negative semidefinite bound on $\dot{W}$ derived in Section III. During the early transient, quadratic current tracking errors dominate, while parameter estimation dynamics govern the slower tail. The tail-averaged sharing errors in Figure 2c remain small and nearly uniform across all buses and DGUs, illustrating that the steady-state sharing equations in the stacked form (9) are independent of individual line parameters once the voltages have converged.

For the PnP scenario (Case 2), Figure 2d shows the per DGU currents at a representative bus. Each plug–in or plug–out event produces a localized transient where the individual currents reallocate to accommodate the new population of DGUs, but the magnitudes remain bounded and quickly reconverge to a new constant sharing profile. This complies with the Lyapunov function where adding or removing DGUs modifies the dimension of the current vector and the weights in (12), but does not alter the sign of $\dot{W}$ or the form of the dissipative terms. The grouped bars in Figure 2e summarize the steady state norms $\|i_{\mathrm{ach}} - i^{\star}\|$ across DGUs on three buses. The bars are clustered close to the horizontal axis, indicating that the residual sharing errors after PnP events remain at the level of numerical precision. The line current envelope in Figure 2f shows that the maximum and typical line currents exhibit only localized bumps at the PnP instants and remain within the same bounded envelope as in the nominal case. This was expected from (9a)–(9b) given bounded voltages and DGU currents and forward invariance of the admissible voltage set.

In the unknown reconfiguration and contingency scenario (Case 3), Figure 2g displays the line current envelope when lines are opened and reclosed without informing the controller. Each topology change induces a sharp but bounded excursion in the envelope, followed by a return to the same steady state level as before the event. Figure 2h tracks the effective edge gains associated with selected lines; the gains exhibit piecewise smooth trajectories that reconfigure when a line is disconnected or reconnected. These trajectories reflect the time–varying structure of the network but do not affect the sign of $\dot{W}$, since the gains do not enter the symmetric skew J terms. Figure 2i shows the time evolution of the adaptive damping coefficients $\kappa_{2,i}(t)$ for selected buses. Each contingency triggers a localized increase in $\kappa_{2,i}(t)$, as prescribed by the design rule (24), which temporarily strengthens the injection–current damping until the voltages and currents have resettled.

V. Conclusion

A fully decentralized nonlinear adaptive backstepping controller has been presented for AC microgrid clusters with

979-8-3315-8138-1

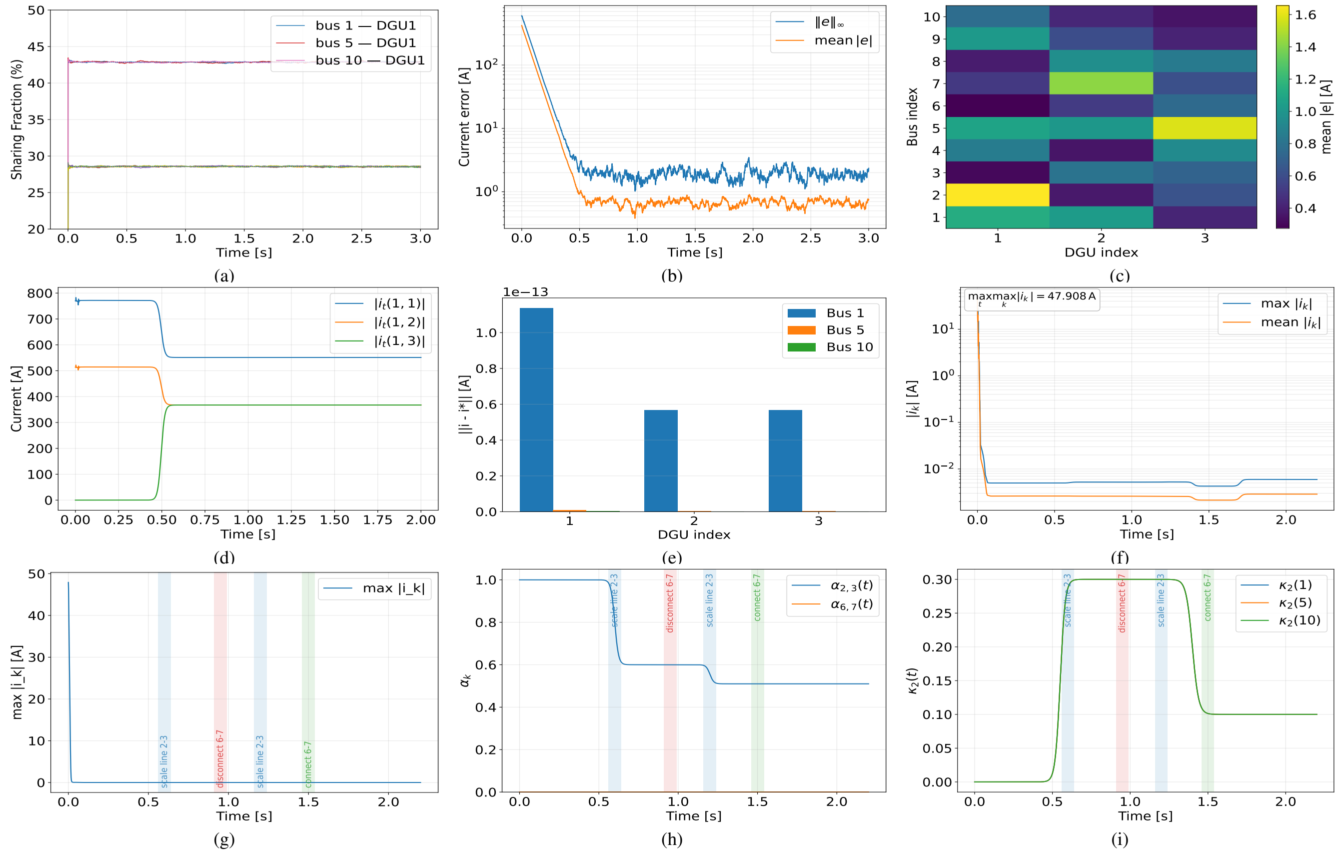

Fig. 2: Performance of the adaptive ZIE controller under proportional current sharing (top row), plug-and-play DGU events (middle row), and unknown line reconfigurations (bottom row).

arbitrary interconnections, unknown network parameters, and nonlinear ZIE loads. Each MG contains multiple parallel DGUs with one grid-forming unit to regulate bus voltage and frequency with grid-feeding units to enforce proportional current/power sharing. The design requires only local measurements, and is independent of the parameters of the distribution-line, enabling robustness to PnP events and line contingencies. A Lyapunov analysis in the dq frame establishes boundedness of all signals and convergence of the desired voltages with accurate sharing, while the adaptive laws identify the aggregated load and network terms online. Future work will investigate a higher-level optimization layers and experimental validation on hardware-in-the-loop MG clusters and extensions to unbalanced three-phase networks with communication delays.

References

[1] J. M. Guerrero, J. C. Vasquez, J. Matas, L. G. De Vicuña, and M. Castilla, "Hierarchical control of droop-controlled ac and dc microgrids—a general approach toward standardization," *IEEE Transactions on Industrial Electronics*, vol. 58, no. 1, pp. 158–172, 2011.

[2] R. H. Lasseter, "Smart distribution: Coupled microgrids," *Proceedings of the IEEE*, vol. 99, no. 6, pp. 1074–1082, 2011.

[3] A. Bidram and A. Davoudi, "Hierarchical structure of microgrids control system," *IEEE Transactions on Smart Grid*, vol. 3, no. 4, pp. 1963–1976, 2012.

[4] M. Tucci, L. Meng, C. Dou, and J. M. Guerrero, "Plug-and-play control of ac microgrids: Achievements and challenges," *IEEE Transactions on Smart Grid*, vol. 10, no. 3, pp. 3069–3077, 2019.

[5] S. Sahoo, P. Siano, S. Doolla, and J. M. Guerrero, "Primary control level voltage and frequency regulation in autonomous microgrids using virtual impedance," *IEEE Transactions on Power Systems*, vol. 34, no. 3, pp. 2369–2379, 2019.

[6] J. Fattahi, H. Schriemer, B. Bacque, R. Orr, K. Hinzer, and J. E. Haysom, "High stability adaptive microgrid control method using fuzzy logic," *Sustainable Cities and Society*, vol. 25, pp. 57–64, 2016.

[7] X. Liu and F. Blaabjerg, "Stability analysis of grid-connected converters interacting with weak grids," *IEEE Transactions on Power Electronics*, vol. 35, no. 5, pp. 4782–4795, 2020.

[8] L. Cheng, X. Fang, and Y. Hu, "Consensus-based distributed control for power sharing and voltage restoration in ac microgrids," *IEEE Transactions on Industrial Informatics*, vol. 17, no. 6, pp. 4169–4180, 2021.

[9] S.-K. Lee, J. Yu, and Y.-S. Kim, "Model predictive control for inverter-based microgrids with voltage and frequency constraints," *IEEE Transactions on Power Systems*, vol. 35, no. 5, pp. 4074–4085, 2020.

[10] M. Tucci, L. Meng, and J. M. Guerrero, "Game-theoretic cooperative control of ac microgrids," *IEEE Transactions on Smart Grid*, vol. 11, no. 4, pp. 3291–3302, 2020.

[11] J. Schiffer, D. Zonetti, R. Ortega, A. M. Stankovic, and J. Raisch, "A survey on modeling of microgrids—from fundamental physics to phasors and voltage sources," *Automatica*, vol. 74, pp. 135–150, 2016.

[12] P. Mandal, D. Das, and C. Chakraborty, "Dynamic load modeling for inverter-based microgrids: A comprehensive review," *IEEE Transactions on Smart Grid*, vol. 12, no. 5, pp. 4255–4268, 2021.

[13] J. Sun, "Impedance-based stability criterion for grid-connected inverters," *IEEE Transactions on Power Electronics*, vol. 26, no. 11, pp. 3075–3078, 2011.

[14] M. Krstić, I. Kanellakopoulos, and P. V. Kokotović, *Nonlinear and Adaptive Control Design*. New York, NY: John Wiley & Sons, 1995.

[15] H. K. Khalil, *Nonlinear Systems*, 3rd ed. Upper Saddle River, NJ: Prentice Hall, 2002.

[16] Y. Wang, L. Xie, and C. E. De Souza, "Robust control of a class of uncertain nonlinear systems," *Syst. Contr. Let.*, vol. 19, no. 2, pp. 139–149, 1992.

979-8-3315-8138-1